Impact of a hydrophobic ion on the early stage of atmospheric aerosol formation

Linda Feketeová[a], Paul Bertier[a,b], Thibaud Salbaing[a], Toshiyuki Azuma[b], Florent Calvo[c], Bernadette Farizon[a], Michel Farizon[a,1], and Tilmann D. Märk[d]

[a]Université de Lyon, Université Claude Bernard Lyon 1, CNRS, Institut National de Physique Nucléaire et de Physique des Particules (IN2P3), Institut de Physique des 2 Infinis de Lyon (IP2I) Lyon, UMR 5822, F-69622 Villeurbanne, France; [b]Atomic, Molecular & Optics (AMO) Physics Laboratory, RIKEN Cluster for Pioneering Research, 351-0198 Saitama, Japan; [c]Université Grenoble Alpes, CNRS, Laboratoire Interdisciplinaire de Physique (LIPhy), 38000 Grenoble, France; and [d]Institut für Lonenphysik und Angewandte Physik, Leopold Franzens Universität, 6020 Innsbruck, Austria

Edited by Paul M. Winkler, University of Vienna, Vienna, Austria, and accepted by Editorial Board Member John D. Weeks October 1, 2019 (received for review June 28, 2019)

Atmospheric aerosols are one of the major factors affecting planetary climate, and the addition of anthropogenic molecules into the atmosphere is known to strongly affect cloud formation. The broad variety of compounds present in such dilute media and their specific underlying thermalization processes at the nanoscale make a complete quantitative description of atmospheric aerosol formation certainly challenging. In particular, it requires fundamental knowledge about the role of impurities in water cluster growth, a crucial step in the early stage of aerosol and cloud formation. Here, we show how a hydrophobic pyridinium ion within a water cluster drastically changes the thermalization properties, which will in turn change the corresponding propensity for water cluster growth. The combination of velocity map imaging with a recently developed mass spectrometry technique allows the direct measurement of the velocity distribution of the water molecules evaporated from excited clusters. In contrast to previous results on pure water clusters, the low-velocity part of the distributions for pyridinium-doped water clusters is composed of 2 distinct Maxwell–Boltzmann distributions, indicating out-of-equilibrium evaporation. More generally, the evaporation of water molecules from excited clusters is found to be much slower when the cluster is doped with a pyridinium ion. Therefore, the presence of a contaminant molecule in the nascent cluster changes the energy storage and disposal in the early stages of gas-to-particle conversion, thereby leading to an increased rate of formation of water clusters and consequently facilitating homogeneous nucleation at the early stages of atmospheric aerosol formation.

out-of-equilibrium dynamics | nanoscale thermodynamics | atmospheric aerosol formation | protonated pyridine | protonated water clusters

Aerosols are tiny atmospheric particles that have a major impact on the Earth's climate. They scatter or absorb sunlight and influence cloud formation through the ability to act as condensation nuclei (1–7). Understanding the mechanisms by which molecules in the gas phase aggregate to form larger particles and eventually aerosols is of key importance to critically assess their role in global climate change (8, 9) and the related public health issues associated with inhalation of ultrafine particles (10). Gas-to-particle conversion also known as secondary aerosol formation has been observed in many areas around the world (11). Particle nucleation is observed to be responsible for about half of the global cloud condensation nuclei and is the dominant source in the free troposphere (12). Nucleation of atmospheric particles is thought to involve both neutral- and ion-induced pathways, in proportions that depend on altitude (13). The presence of ions has been predicted to enhance the growth rates of nanometer-size aerosol particles (14–16). Recently, it was shown by Fan et al. (4) that anthropogenic ultrafine aerosol particles smaller than 50 nm may have a stronger influence on cloud formation than previously believed. However, and despite extensive research, the early stages governing the atmospheric aerosol nucleation remain uncertain. Many experiments to date have focused on the nature of the main compounds and their possible role involved in the nucleation processes. Originally, binary homogeneous nucleation of sulfuric acid and water was thought to be the dominant process; nevertheless the binary results involving these species alone cannot explain the nucleation rates and growth rates observed in the atmosphere (17, 18). Subsequently, ternary homogeneous nucleation involving ammonia, sulfuric acid, and water was shown to increase significantly the nucleation and growth rates (3, 18, 19). More recently, further experiments demonstrated that amines such as dimethylamine (DMA) enhance even more the neutral and ion-induced H_2SO_4/H_2O nucleation in the atmosphere (20, 21). Moreover, according to Vaida (22) the presence of water clusters in the atmosphere facilitates the nucleation processes by increasing the effective cross-section and the interaction time between the 3 species (23). Therefore, water cluster production is of relevance in this context and its details have to be considered to elucidate the overall nucleation process, in particular condensation and subsequent evaporation processes.

At the molecular level, condensation and evaporation from a bulk water surface are statistical phenomena: For a large number of molecules, and as a result of energy equipartitioning at thermal equilibrium, evaporation manifests itself in a Maxwell–Boltzmann

Significance

Gas-to-particle conversion, also known as atmospheric aerosol nucleation, is responsible for about half of the global cloud condensation nuclei. It has been further argued that homogenous ternary nucleation including water is the major pathway for atmospheric aerosol formation. In contrast to earlier results on pure protonated water clusters, the shape of the measured velocity distributions of water molecules evaporated from excited water clusters doped with pyridinium, an abundant anthropogenic ion in the troposphere, shows evidence for out-of-equilibrium evaporation prior to thermalization. Water molecule evaporation is found to be much slower for the doped clusters, indicating in turn how such contaminants facilitate the growth of water clusters and consequently the nucleation processes at the early stages of atmospheric aerosol formation.

Author contributions: B.F., M.F., and T.D.M. designed research; L.F., P.B., F.C., B.F., and M.F. performed research; P.B., T.S., F.C., and M.F. contributed new reagents/analytic tools; L.F., P.B., T.S., and M.F. analyzed data; and L.F., T.A., F.C., B.F., M.F., and T.D.M. wrote the paper.

The authors declare no competing interest.

This article is a PNAS Direct Submission. P.M.W. is a guest editor invited by the Editorial Board.

[1]To whom correspondence may be addressed. Email: m.farizon@ipnl.in2p3.fr.

This article contains supporting information online at www.pnas.org/lookup/suppl/doi:10.1073/pnas.1911136116/-/DCSupplemental.

First published October 21, 2019.

(MB) velocity distribution for the evaporated molecules (24). In small water clusters with few degrees of freedom, evaporation competes more strongly with energy redistribution upon excitation after condensation and different velocity distributions may arise. To elucidate this phenomenon on a microscopic level, molecular evaporation from ultimately small protonated water clusters containing less than 10 molecules was investigated using a recently developed experimental technique (25, 26). After a femtosecond excitation induced by a single high-velocity collision with an argon atom, the out-of-equilibrium water cluster ion relaxes via the evaporation of 1 or several molecules. The measured velocity distributions of the molecules evaporated from $(H_3O^+)(H_2O)_n$ protonated water clusters for $n = 1$ to 10 exhibit 2 contributions, namely a low-velocity part that can be well described by MB statistics and a high-velocity part corresponding to nonergodic (NE) events caused by molecules that evaporate before complete redistribution of the excitation energy within the cluster. Through dedicated atomistic modeling based on statistical molecular dynamics (SMD) simulations (26, 27), the statistical nature of the main contribution at low velocities and the sequential evaporation of several molecules were confirmed by the ability to reproduce the experimental velocity distributions (28). Moreover, the contribution of NE events observed at high velocities was analyzed and interpreted as being due to the evaporation of molecules before complete redistribution of the excitation energy.

In the present work, we address the thermalizing ability of water cluster ions containing a hydrophobic ion, namely pyridinium (PyH^+), upon sudden excitation of one of its molecules. Pyridine is an example of molecules present in the Earth's atmosphere due to human activity and is likely involved in aerosol particle condensation processes (29–32). Pyridinium has been shown to be by far the most abundant core ion in the troposphere (30, 31, 33, 34). It also has been observed in the positive-ion mass spectra obtained in the CLOUD chamber experiments at CERN; however, pyridine was considered to be a nonactive molecule like other impurities in the aerosol formation process (21). Here we argue that after all pyridine may have a decisive effect of catalytic nature in atmospheric aerosol formation due to its different behavior when replacing a hydronium ion with a pyridinium ion in a nascent water cluster.

Results and Discussion

The velocity distributions measured for the evaporation of 1 water molecule from $(PyH^+)(H_2O)_n$ (shown in Fig. 1*A* for $n = 4$) exhibit 2 distinct components, as observed previously for pure water clusters (26). However, in contrast to the latter case, the low-velocity part of the distribution presently measured for single-molecule evaporation cannot be satisfactorily fitted by a single MB distribution. Similarly, the low-velocity part of the distribution measured for the evaporation of 2 or 3 water molecules from $(PyH^+)(H_2O)_n$ cannot be reproduced by Monte Carlo (MC) simulations as in the pure water case, assuming 1) sequential single-molecule evaporation from protonated water clusters and 2) the use of the low-velocity part of the velocity distribution measured for single-molecule evaporation from a protonated water cluster with $n = 4$, 3, and 2 water molecules as a starting point for the calculations (*SI Appendix*, Fig. S1). Therefore, to elucidate this drastically different behavior, SMD simulations were performed for $(PyH^+)(H_2O)_n$ assuming, as for pure water clusters, that any of the $n + 1$ molecular units of the water cluster, including the pyridinium ion, can carry the initial excitation. The velocity distributions thus obtained are shown in Fig. 1 *B–D* for $(PyH^+)(H_2O)_4$. Assuming in these simulations that the local excitation resides in the pyridinium ion, a single MB distribution without any NE event is obtained. In contrast, assuming local excitation of a random water molecule produces both types of contributions, i.e., an MB distribution appearing at low velocities and a distinct contribution at higher velocities, in

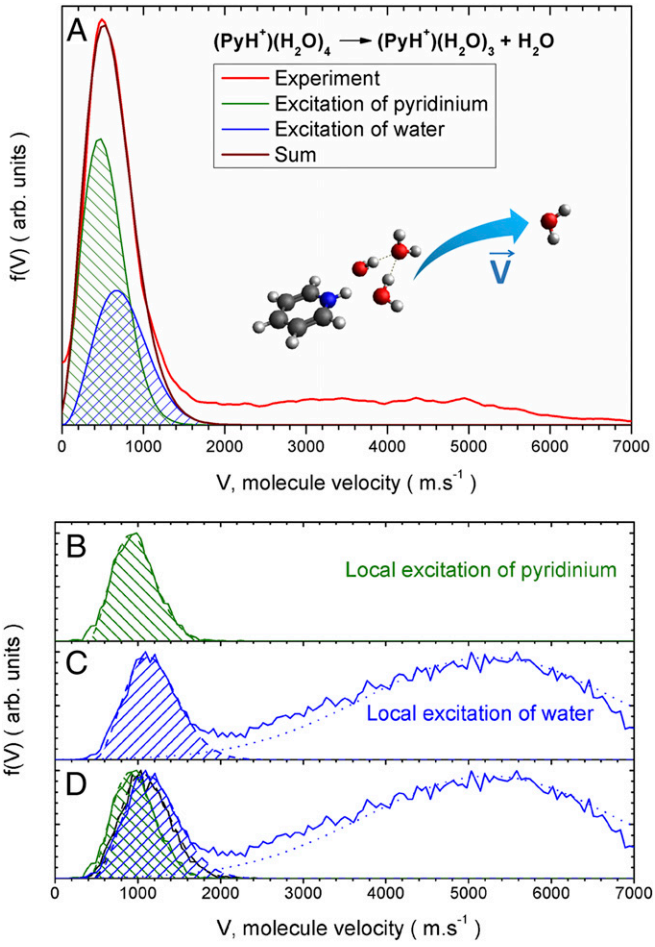

Fig. 1. Velocity distribution of water molecules evaporated from $(PyH^+)(H_2O)_4$. (*A*) Measured velocity distribution (red curve) and 2 calculated MB contributions corresponding to the local excitation of a water molecule (blue curve) or the pyridinium ion (green curve), whose sum is also represented (brown curve). The relative weights of the 2 contributions were obtained by fitting the experimental data with the calculated MB distributions shown in *B* and *C*, yielding 63% in the case of local excitations on pyridinium and 37% on water. *B–D* show the SMD simulation results, i.e., the velocity distributions obtained upon local excitation of (*B*) the pyridinium ion or (*C*) a random water molecule; (*D*) these 2 distributions are compared to the distribution obtained if the excitation is assumed to be uniformly distributed on all molecules (black curve). The 2 MB distributions obtained for local excitation are shifted in opposite directions compared to the calculated distribution corresponding to the complete thermalization of the cluster (black curve).

accordance with the results observed earlier for pure water clusters (26). Additionally, the velocity distribution obtained by assuming the initial excitation to be uniformly distributed among all atoms of the water cluster exhibits an MB distribution that corresponds neither to that obtained for local excitation of the pyridinium ion nor to that obtained for local excitation of a water molecule. Interestingly, the most important feature compared to the pure water cluster case is the observed shift of the MB contribution, depending on the type of molecular unit chosen to initially carry the excitation energy. As seen in Fig. 1*D*, the water molecules evaporate with lower velocities on average when the initial excitation is localized on the pyridinium ion, whereas excitations localized on a random water molecule result in evaporated molecules with higher velocities. Taking these 2 initial excitation possibilities into account in the experimental dataset, the low-velocity part of the experimental distribution measured for single water molecule evaporation can be very well fitted by these 2 types of MB

distributions (Fig. 1*A*), fixing the widths of the distributions and the shift between them based on the SMD results. In contrast to the results observed earlier for pure water (26), the low-velocity part of the distribution in the contaminated case is affected by the presence of this impurity and the 2 MB components demonstrate the evaporation of a water molecule before thermalization of the entire water cluster. In the experiment, the relative contributions of MB and NE events amount to 63% versus 37% for $n = 4$ in Fig. 1*A*. This ratio does not match the values of the simple cross-sections of the pyridinium and water subparts of the nanodroplet that would be obtained from the geometric positions (42% versus 58%) or the ground-state electronic density (38% versus 62% from a DFT/B3LYP/6-311+G* calculation). This confirms that energy redistribution upon collision with the argon atom is a more complex process involving also electronic excited states. In the SMD simulations, the observed ratio is meaningless because, unlike in the experiment, the probability of exciting any specific molecule is fixed as a constant.

The presence of 2 MB components in the low-velocity part of the velocity distribution is observed not only for $n = 4$ but also for the smaller sizes of the water clusters, $n = 1$ to 3. To compare this low-velocity contribution of the experimental distributions with those measured under the same experimental conditions for pure water $(H_3O^+)(H_2O)_{n=1–10}$ water clusters, their mean value $\langle V \rangle$ and their full width at half maximum ΔV were determined. As shown in Fig. 2, for $n = 1$ to 4, both $\langle V \rangle$ and ΔV are larger for pure water clusters than for the doped water clusters, indicating that, on average, less energy is available for water evaporation in doped water clusters. To understand this difference, we note that an initial excitation of the pyridinium impurity must be transferred to the water part of the cluster to later trigger water molecule evaporation. Since the pyridinium ion is hydrophobic, energy transfer to water is restricted to a few intermolecular bonds and will thus be much slower than in the case of a hydronium ion that is fully solvated by all water molecules in a pure water cluster. This bottleneck in the energy transfer gives rise to much slower redistribution rates, a result that is confirmed by SMD calculations in which the time correlation function of the kinetic energy initially deposited in the pyridinium ion exhibits a decay rate of the order of tens of picoseconds, while the same quantity in the hydronium ion in the pure water cluster decays over not even a picosecond (Fig. 3). The present results therefore confirm that water molecule evaporation can occur much faster than the time needed for complete thermalization, including energy transfer from the excited impurity. From the Maxwell–Boltzmann distributions presented in Fig. 1*A* (red curve) an effective translational temperature T can be extracted using the value of the most probable velocity v_p, which according to the kinetic theory of gases are related to one another via

$$v_p = \sqrt{\frac{2k_BT}{m}}, \qquad [1]$$

where k_B is the Boltzmann constant and m the mass of a water molecule. This effective temperature is found to vary from ~2,800 K down to ~300 K with increasing size n for protonated water clusters (36) and from ~600 K down to ~300 K for pyridinium–water clusters. As shown by McGraw and Laviolette (37) in the context of classical nucleation theory, temperature fluctuations can markedly influence evaporation and nucleation rates, although such effects remain limited for systems containing hundreds of particles. The broader fluctuations reported here, which are due to both stronger size effects and the delayed energy redistribution from pyridine to water, could thus have a greater influence.

Our analysis of the measured velocity distributions for single-molecule evaporation from excited contaminated water clusters

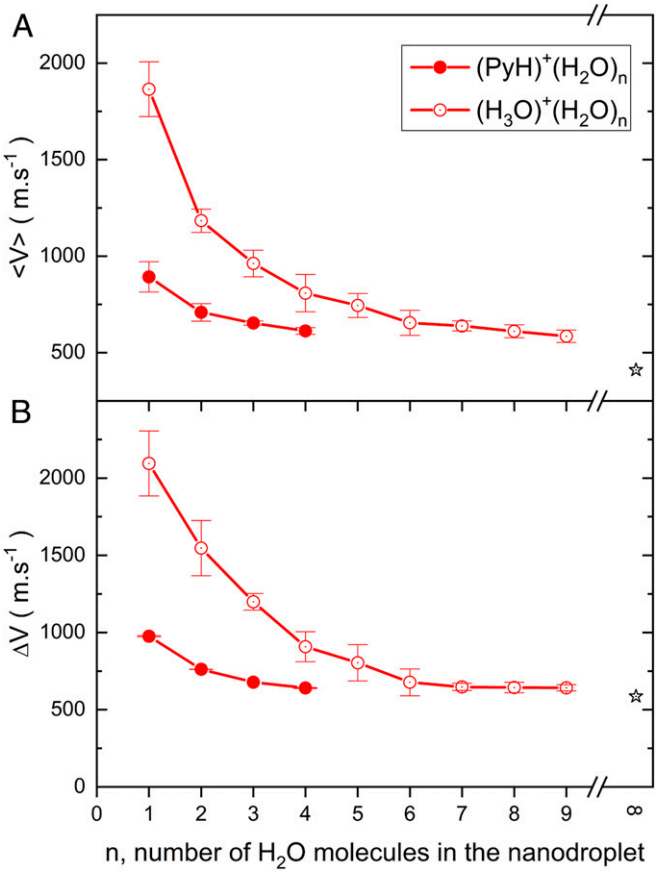

Fig. 2. Mean value and full width at half maximum of the evaporated H_2O velocity distribution versus the number of H_2O molecules in the cluster. (*A* and *B*) Experimental (*A*) mean values $\langle V \rangle$ and (*B*) full widths at half maximum ΔV of the H_2O velocity distributions for $(PyH^+)(H_2O)_{n=1–4}$ are shown as solid circles and for $(H_3O^+)(H_2O)_{n=1–10}$ as open circles. The value in the limit of infinitely large systems (gray star) was obtained from a bulk simulation by Varilly and Chandler (35).

provides evidence that the velocity distribution of the evaporated water molecules contains fingerprints of where the energy was initially deposited. Such features, including the occurrence of a 2-component MB distribution for single evaporation, are further confirmed by considering the sequential evaporation of several molecules from the excited water cluster. Using the MB distributions originating from the excitation of either the pyridinium ion or a water molecule separately as a starting point in an MC simulation, the resulting distributions exhibit distinct shifts (*SI Appendix*, Fig. S2), clearly moving toward lower velocity values for pyridinium ion excitation compared to cases where a water molecule is excited. These calculated distributions reproduce the low-velocity part of the distribution measured for the evaporation of 2 and 3 water molecules very well, as shown in Fig. 2 in the case of 2-molecule evaporation. Moreover, as shown in Fig. 1*A*, the excitation of the pyridinium ion is found to give the major contribution to the single-molecule evaporation during the observational time window, excluding NE events. In contrast, and as shown in Fig. 4, the evaporation of 2 molecules more likely originates from the local excitation of a water molecule. This result is in agreement with the much longer time required to transfer energy from pyridinium to water through the hydrophobic bottleneck, whereas energy redistribution is much faster within the water components.

These considerations inferred from the present experimental results are of direct relevance for the atmospheric aerosol nucleation

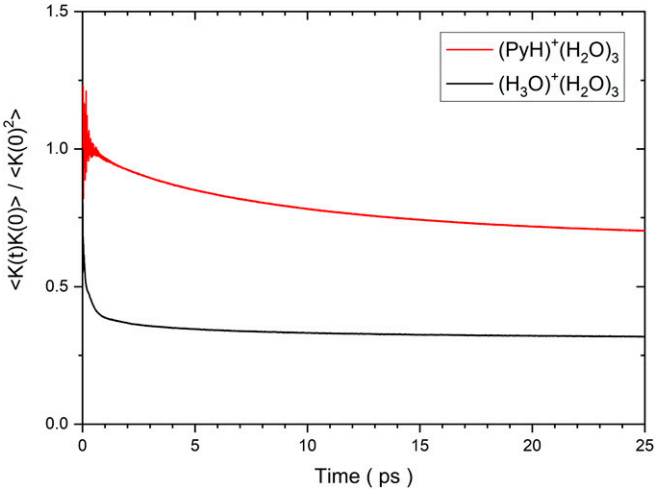

Fig. 3. Relaxation times of the energy deposited in the molecular ion. Shown are time correlation functions of the global kinetic energy in $(PyH^+)(H_2O)_3$ and $(H_3O^+)(H_2O)_3$ upon excitation of the cationic molecule at time $t = 0$, as obtained from molecular dynamics simulations and showing the very different relaxation times of energy transfer in the 2 systems.

processes. The translational energy transferred by a condensing water molecule impinging on the pyridinium site of the cluster is not immediately available for water molecule evaporation, allowing a more efficient cluster growth. As the number of water molecules increases, the amount of energy that can be stored in the water subpart increases with the number of vibrational modes, and the role of the pyridinium ion eventually vanishes. Considering the relative proton affinities of pyridine and water, the extra proton should switch to the water subpart to form a hydronium ion when the cluster is large enough (38). Then, the resulting neutral pyridine molecule will evaporate easily, becoming available for further nucleation processes by interaction with another hydronium ion. Atmospheric pyridine and pyridine derivatives are believed to originate from biomass burning, automobile exhaust, coal tars, and tobacco smoke (ref. 29 and references therein). The main atmospheric sink is considered to be reactions with OH radicals (29–32, 39). The estimated atmospheric lifetime of pyridine based on experimentally determined reaction rate coefficients may range from 23 to 46 days (29, 39). Taking into account the present results it is thus very likely that a single pyridine molecule could be involved in multiple ion-induced nucleation events during its lifetime in the troposphere. Therefore, replacing initially the hydronium ion by a pyridinium ion facilitates water cluster formation and consequently processes at the early stages of atmospheric aerosol formation.

The present quantitative measurements and their results should contribute to bridging the knowledge gap between out-of-equilibrium dynamics of water at the nanoscale and our understanding of atmospheric aerosol formation and especially its implications in the modeling of climate evolution on a more global scale (7). These insights into the out-of-equilibrium dynamics of ultimately small protonated water clusters doped with a hydrophobic impurity shed further light on the decisive influence of contaminating molecules in the atmosphere and their crucial role in aerosol and cloud formation.

Materials and Methods

Experimental. The DIAM (Device for Irradiation of Molecular Clusters, Dispositif d'Irradiation d'Agrégats Moléculaires) apparatus used for the generation of mass- and energy-selected beams of molecular cluster ions has been described in detail elsewhere (40). Briefly, doped water clusters were produced by electron impact after supersonic expansion of water and pyridine vapor seeded in helium. The doped clusters, $(PyH^+)(H_2O)_{n=2-4}$, containing a given number of water molecules n were mass and velocity selected by a double-focusing 2-sector field mass spectrometer more than 1 ms after being formed (40). A single high-velocity collision (with velocity in the laboratory frame ranging from 10^5 to 2.10^5 $m{\cdot}s^{-1}$) with an argon atom led to energy deposition in the droplet via electronic excitation (41–43) of one of the water molecules or of the pyridinium ion on a femtosecond timescale (44).

As previously considered for protonated water clusters such high-velocity collisions (45, 46) corresponded to a broad range of energy deposition from 0 to 12 eV (80% below 4 eV) (47), and therefore, on average, the energy deposited was much higher than the binding energy of a molecule in the droplet. After excitation, the out-of-equilibrium cluster relaxed through evaporation of one or several molecules. The protonated residue was mass analyzed at least 200 ns after the collision in a specially designed time-of-flight and velocity map imaging apparatus. After fragmentation, the charged species were accelerated by 1.8 kV before reaching a field-free zone, whereas the neutral fragments nearly maintained the initial velocity of the parent ion. The charged fragments reached the microchannel plate detector (MCP) significantly earlier than the neutral species. For each dissociated cluster, the correlation between the arrival times of the charged and neutral fragments was recorded. The impact position was measured with a delay line anode placed behind the MCP.

The total kinetic energy released (KER) during dissociation was partitioned owing to momentum conservation; i.e., the evaporated molecules acquired an additional velocity randomly oriented in the center-of-mass reference frame of the parent droplet, which resulted in a characteristic change in the impact position within the detection plane. Measurements combining velocity map imaging with the correlated ion and a neutral time-of-flight mass spectrometry technique (COINTOF MS) (25, 26, 48–52) were performed on an event-by-event basis for a large number of individual droplets (typically 10^6). The event-by-event analysis of the recorded data was performed in the ROOT software framework (53).

Atomistic Simulations. SMD trajectories were performed to simulate the evaporation of $(PyH^+)(H_2O)_{n=2-4}$ clusters initially thermalized at 100 K and undergoing a sudden excitation either localized on 1 random molecule or distributed uniformly on all atoms. The Amber ff94 force field (54) was used to describe intermolecular and intramolecular bonding, and a sample of 10^5 phase space configurations was generated at thermal equilibrium using the Nosé–Hoover method. Each SMD individual trajectory correspond to 1 random configuration drawn from this sample and a collision energy in the range of 3 to 8 eV to be deposited as kinetic energy into the entire system or on a subset of atoms corresponding to 1 random water molecule or the pyridinium impurity. The collisional excitation energy was added as kinetic

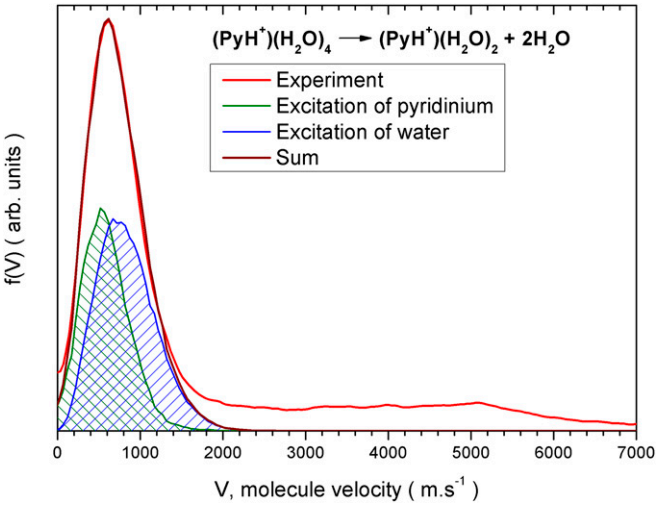

Fig. 4. Evaporation of 2 water molecules from $(PyH^+)(H_2O)_4$. Shown are experimentally measured velocity distributions when 2 molecules evaporate from $(PyH^+)(H_2O)_4$. The calculated distributions assuming a local excitation of the pyridinium ion (in green) or a random water molecule (in blue) and a weighted sum of these 2 cases (in brown) are also shown. The relative weights of these distributions were obtained by fitting the results from an MC simulation of sequential evaporation, yielding a weight of 48% for the pyridinium local excitation.

energy, ensuring that no spurious total linear or angular momenta were created. The trajectory was then propagated without the thermostat. After 1 ns, the fragments were identified from the bond connectivity, and the velocity of each evaporating water molecule was determined. A total of 100,000 independent SMD trajectories were obtained for each cluster size and for localized or uniform excitations.

Additional molecular dynamics trajectories were generated to evaluate the (classical) rate of kinetic energy transfer between the pyridinium ion and the rest of the cluster upon local excitation of the impurity. Here, the variations in the global kinetic energy $K(t)$ of the entire system were monitored as a function of time, from which the time correlation function provided an estimate of the energy transfer rate constant. Similar simulations were performed for the $(H_3O^+)(H_2O)_3$ protonated water cluster, where the hydronium molecule acts as a hydrophilic impurity.

ACKNOWLEDGMENTS. This work was supported by the Agence Nationale de la Recherche Française through Grants ANR-06-BLAN-0319 and ANR-10-BLAN-0411, by the Laboratory of Excellence Lyon Institute of Origins Lyon Institute of Origins (ANR-10-LABX-0066) of the Université de Lyon, by the Groupement de Recherche Edifices Moléculaires Isolés et Environnés GDR 3533, by the joint France Japan Particle Physics laboratory (FJPPL), and by la Mission pour les Initiatives Transverses et Interdisciplinaires (MITI CNRS). We acknowledge the Institut de Physique des 2 Infinis de Lyon (IP2I) for technical support, particularly Raphaël Fillol and Roger Genre. We acknowledge the Centre de Calcul de l'Institut National de Physique Nucléaire et de Physique des Particules (CCIN2P3) for their support and particularly Pascal Calvat and Yonny Cardenas. We thank Prof. Armin Hansel from the Institut für Ionenphysik und Angewandte Physik of the University of Innsbruck for helpful discussions.

1. U. Lohmann, Possible aerosol effects on ice clouds via contact nucleation. *J. Atmos. Sci.* **59**, 647–656 (2002).
2. D. Stolzenburg *et al*., Rapid growth of organic aerosol nanoparticles over a wide tropospheric temperature range. *Proc. Natl. Acad. Sci. U.S.A.* **115**, 9122–9127 (2018).
3. J. Almeida *et al*., Molecular understanding of sulphuric acid-amine particle nucleation in the atmosphere. *Nature* **502**, 359–363 (2013).
4. J. Fan *et al*., Substantial convection and precipitation enhancements by ultrafine aerosol particles. *Science* **359**, 411–418 (2018).
5. H. Gordon *et al*., Reduced anthropogenic aerosol radiative forcing caused by biogenic new particle formation. *Proc. Natl. Acad. Sci. U.S.A.* **113**, 12053–12058 (2016).
6. C. Frege *et al*., Influence of temperature on the molecular composition of ions and charged clusters during pure biogenic nucleation. *Atmos. Chem. Phys.* **18**, 65–79 (2018).
7. Y. Sato *et al*., Aerosol effects on cloud water amounts were successfully simulated by a global cloud-system resolving model. *Nat. Commun.* **9**, 985 (2018).
8. M. Kulmala, Atmospheric science. How particles nucleate and grow. *Science* **302**, 1000–1001 (2003).
9. R. Zhang, A. Khalizov, L. Wang, M. Hu, W. Xu, Nucleation and growth of nanoparticles in the atmosphere. *Chem. Rev.* **112**, 1957–2011 (2012).
10. A. Saxon, D. Diaz-Sanchez, Air pollution and allergy: You are what you breathe. *Nat. Immunol.* **6**, 223–226 (2005).
11. M. Kulmala *et al*., Direct observations of atmospheric aerosol nucleation. *Science* **339**, 943–946 (2013).
12. J. Merikanto *et al*., Impact of nucleation on global CCN. *Atmos. Chem. Phys.* **9**, 8601–8616 (2009).
13. S. H. Lee *et al*., Particle formation by ion nucleation in the upper troposphere and lower stratosphere. *Science* **301**, 1886–1889 (2003).
14. F. Yu, R. P. Turco, Ultrafine aerosol formation via ionmediated nucleation. *Geophys. Res. Lett.* **27**, 883–886 (2000).
15. A. Lushnikov, M. Kulmala, A new flux-matching theory of particle charging. *Eur. Phys. J. D* **29**, 345–355 (2004).
16. P. M. Winkler *et al*., Heterogeneous nucleation experiments bridging the scale from molecular ion clusters to nanoparticles. *Science* **319**, 1374–1377 (2008).
17. M. Kulmala, A. Laarsonen, Binary nucleation of water–sulfuric acid system: Comparison of classical theories with different H_2SO_4 saturation vapor pressures. *J. Chem. Phys.* **93**, 696–701 (1990).
18. J. Kirkby *et al*., Role of sulphuric acid, ammonia and galactic cosmic rays in atmospheric aerosol nucleation. *Nature* **476**, 429–433 (2011).
19. P. Korhonen *et al*., Ternary nucleation of H2SO4, NH3 and H2O in the atmosphere. *J. Geophys. Res.* **104**, 349-26–353-26 (1999).
20. A. Kürten *et al*., Neutral molecular cluster formation of sulfuric acid-dimethylamine observed in real time under atmospheric conditions. *Proc. Natl. Acad. Sci. U.S.A.* **111**, 15019–15024 (2014).
21. F. Bianchi *et al*., Insight into acid-base nucleation experiments by comparison of the chemical composition of positive, negative, and neutral clusters. *Environ. Sci. Technol.* **48**, 13675–13684 (2014).
22. V. Vaida, Perspective: Water cluster mediated atmospheric chemistry. *J. Chem. Phys.* **135**, 020901 (2011).
23. T. D. Märk *et al*., New gas phase inorganic ion cluster species and their atmospheric implications. *Nature* **285**, 392–393 (1980).
24. J. S. Rowlinson, The Maxwell–Boltzmann distribution. *Mol. Phys.* **103**, 2821–2828 (2005).
25. F. Berthias *et al*., Measurement of the velocity of neutral fragments by the "correlated ion and neutral time of flight" method combined with "velocity-map imaging". *Rev. Sci. Instrum.* **88**, 083101 (2017).
26. H. Abdoul-Carime *et al*., Velocity of a molecule evaporated from a water nanodroplet: Maxwell–Boltzmann statistics versus non-ergodic events. *Angew. Chem. Int. Ed. Engl.* **54**, 14685–14689 (2015).
27. F. Calvo *et al*., Collision-induced evaporation of water clusters and contribution of momentum transfer. *Eur. Phys. J. D* **71**, 110 (2017).
28. F. Berthias *et al*., Sequential evaporation of water molecules from protonated water clusters: Measurement of the velocity distributions of the evaporated molecules and statistical analysis. *Phys. Chem. Chem. Phys.* **20**, 18066–18073 (2018).
29. M. J. Ryding, Å. M. Jonsson, A. S. Zatula, P. U. Andersson, E. Uggerud, Reactions of $H^+(pyridine)_m(H_2O)_n$ and $H^+(NH_3)_1(pyridine)_m(H_2O)_n$ with NH_3. *Atmos. Chem. Phys.* **12**, 2809–2822 (2012).
30. F. L. Eisele, First tandem mass spectrometric measurement of tropospheric ions. *J. Geophys. Res.* **93**, 716–724 (1988).
31. P. Schulte, F. Arnold, Pyridinium ions and pyridine in the free troposphere. *Geophys. Res. Lett.* **17**, 1077–1080 (1990).
32. G. Beig, G. P. Brasseur, Model of tropospheric ion composition: A first attempt. *J. Geophys. Res. Atmos.* **105**, 22671–22684 (2000).
33. D. M. Murphy *et al*., Single-particle mass spectrometry of tropospheric aerosol particles. *J. Geophys. Res.* **111**, D23S32 (2006).
34. C. Frege *et al*., Chemical characterization of atmospheric ions at the high altitude research station Jungfraujoch (Switzerland). *Atmos. Chem. Phys.* **17**, 2613–2629 (2017).
35. P. Varilly, D. Chandler, Water evaporation: A transition path sampling study. *J. Phys. Chem. B* **117**, 1419–1428 (2013).
36. F. Berthias *et al*., Maxwell-Boltzmann versus non-ergodic events in the velocity distribution of water molecules evaporated from protonated water nanodroplets. *J. Chem. Phys.* **149**, 084308 (2018).
37. R. McGraw, R. A. Laviolette, Fluctuations, temperature, and detailed balance in classical nucleation theory. *J. Chem. Phys.* **102**, 8983–8994 (1995).
38. F. Berthias *et al*., Proton migration in clusters consisting of protonated pyridine solvated by water molecules. *Chem. Phys. Chem.* **16**, 3151–3155 (2015).
39. R. Atkinson *et al*., Atmospheric chemistry of aniline, N,N-dimethylaniline, pyridine, 1,3,5-triazine, and nitrobenzene. *Environ. Sci. Technol.* **21**, 64–72 (1987).
40. G. Bruny *et al*., A new experimental setup designed for the investigation of irradiation of nanosystems in the gas phase: A high intensity mass-and-energy selected cluster beam. *Rev. Sci. Instrum.* **83**, 013305 (2012).
41. H. S. Lee, M. J. Kim, Excitation mechanism in the collision-induced dissociation of methane molecular ion at kiloelectronvolt translational energy. *J. Phys. Chem.* **100**, 1459–1465 (1996).
42. R. G. Cooks, Special feature: Historical. Collision-induced dissociation: Readings and commentary. *J. Mass Spectrom.* **30**, 1215–1221 (1995).
43. U. Saalmann, R. Schmidt, Excitation and relaxation in atom-cluster collisions. *Phys. Rev. Lett.* **80**, 3213–3216 (1998).
44. F. Remacle, R. D. Levine, An electronic time scale in chemistry. *Proc. Natl. Acad. Sci. U.S.A.* **103**, 6793–6798 (2006).
45. B. Liu *et al*., Collision-induced dissociation of hydrated adenosine monophosphate nucleotide ions: Protection of the ion in water nanoclusters. *Phys. Rev. Lett.* **97**, 133401 (2006).
46. H. Da Silva *et al*., Multiple electron capture, excitation, and fragmentation in C^{6+} - C_{60} collisions. *Phys. Rev. A* **89**, 032701 (2014).
47. S. Hayakawa, A. Kitaguchi, S. Kameoka, M. Toyoda, T. Ichihara, Differences between the internal energy depositions induced by collisional activation and by electron transfer of W(CO)6(2+) ions on collision with Ar and K targets. *J. Chem. Phys.* **124**, 224320 (2006).
48. F. Berthias *et al*., Collision-induced dissociation of protonated water clusters. *Phys. Rev. A* **89**, 062705 (2014).
49. M. Farizon *et al*., "Method for tandem time of flight analysis and analysis appliance using said method." Patent PCT/FR2010/052733 (2009).
50. M. Farizon *et al*., "Method for tandem time of flight analysis and analysis appliance using said method." Patent WO 2011/080455 (2011).
51. C. Teyssier *et al*., A novel "correlated ion and neutral time of flight" method: Event-by-event detection of neutral and charged fragments in collision induced dissociation of mass selected ions. *Rev. Sci. Instrum.* **85**, 015118 (2014).
52. F. Berthias *et al*., Correlated ion and neutral time of flight technique combined with velocity map imaging: Quantitative measurements for dissociation processes in excited molecular nano-systems. *Rev. Sci. Instrum.* **89**, 013107 (2018).
53. I. Antcheva *et al*., ROOT — A C^{++} framework for petabyte data storage, statistical analysis and visualization. *Comput. Phys. Commun.* **180**, 2499–2512 (2009).
54. J. Wang, P. Cieplak, K. A. Kollman, How well does a restrained electrostatic potential (RESP) model perform in calculating conformational energies of organic and biological molecules? *J. Comput. Chem.* **21**, 1049–1074 (2000).